Volume 14, Number 5, 2021. pp. 437-444

Jordan Journal of Physics

ARTICLE

Albumen-assisted Synthesis of Nanocrystalline Nickel Ferrite Photocatalyst

P. Aji Udhaya[a,b], **M. Meena**[c], **M. Abila Jeba Queen**[a], **M. Mary Freeda**[a] and **T. Regin Das**[d]

[a] *Department of Physics, Holy Cross College, Nagercoil, Affiliated to Manonmaniam Sundaranar University, Abishekapatti, Tirunelvel-627012, India.*

[b] *Research Scholar, Reg. No. 18123152132038, Department of Physics, S.T. Hindu College, Nagercoil, Affiliated to Manonmaniam Sundaranar University, Abishekapatti, Tirunelvel-627012, India.*

[c] *Department of Physics, S.T. Hindu College, Nagercoil, Affiliated to Manonmaniam Sundaranar University, Abishekapatti, Tirunelvel-627012, India.*

[d] *Department of Physics, Lekshmipuram Arts and Science College, Neyyoor, Nagercoil, India.*

Doi: **https://doi.org/10.47011/14.5.5**

Received on: 01/05/2020; *Accepted on: 15/09/2020*

Abstract: As a simple step to remove the polluting dyes in aqua ecosystem, $NiFe_2O_4$ nanoparticles well known for their ferromagnetic properties, low conductivity and high electrochemical stability were prepared by simple auto combustion method using egg white as fuel *via* green synthesis route. The structural, morphological and magnetic properties of prepared $NiFe_2O_4$ was analyzed. The desirable phase purity of the prepared spinel ferrite was deliberated by X-ray Diffractometer (XRD), Fourier Transform Infrared Spectrometer (FTIR), Scanning Electron Microscopy (SEM), Energy Dispersive and Vibrating Sample Magnetometer (VSM). XRD predicts the phase formation, particle size and lattice parameter of the spinel ferrite. The FTIR spectrum confirms the ferrite structure. The morphological and elemental analysis was made using SEM and EDAX. The hysteresis curve reveals the magnetic properties, such as remanence magnetization (Mr), coercivity (H_c) and saturation magnetization (M_s). The photocatalytic efficiency of the synthesized samples was determined from degradation of methylene blue dye. The whole process was monitored using spectrophotometer at regular intervals of time. The maximum photocatalytic degradation efficiency for $NiFe_2O_4$ is around 95.6 %.

Keywords: $NiFe_2O_4$, Ferrite, Green synthesis, Egg white, Combustion, Photocatalyst.

1. Introduction

Wastewater management in developing countries is a major problem due to various industrial processes that meet human needs. Dyeing and pigment industries are of major environmental concern among the various industries, as wastewater includes several non-biodegradable organic colors. From textiles to food, dyes are widely used by humans. Methylene blue is an organic dye that is synthetic and water soluble. It is widely used as a colorant in textiles, paper, plastics, cosmetics, leather, food and many other industries, leading to large dye effluent discharges. If the effluents are not treated properly, they become a serious environmental problem that affects the flora and fauna, as well as human health. Methylene blue dye can irradiate the eyes and skin and damage the respiratory, reproductive, and nervous systems through carcinogenic actions. In

Corresponding Author: P. Aji Udhaya **Email**: ajiudhaya@gmail.com

addition, Methylene blue is dangerous even at very low concentrations and therefore, methylene blue effluent treatment becomes more vital [1].

For the treatment of methylene blue-containing water, techniques such as photocatalytic degradation, ozonation, electrochemical method, Fenton process and so on were employed. In the present day, photocatalysis is preferred over other methods of treatment for color degradation, as light irradiation generates pairs of electrons and holes on a semiconductor. The photogenerated hole (h^+) reacts in aqueous solution with H_2O and OH^- to form hydroxyl radical (OH^-), which is a key and effective oxidizing agent for the degradation of such a toxic dye [2].

Ferrites are ferrimagnetic materials encompassing complex oxides composed of oxides comprising ferric ions as the main constituent and classified as magnetic materials as they parade ferrimagnetic behavior. The magnetic chattels of ferrite rise from interactions amid metallic ions inhabiting particular positions comparative to the oxygen ions in the crystal structure of the oxide. Snoek and his associates advanced assortment of ferrites during 1945 to 1993 at the Philips Research Laboratories, Netherland.

Based on the molar ratio of Fe_2O_3 to other oxide components present in them and their crystal structure, ferrites can further be classified into four different groups as spinel ferrites, garnet ferrites, ortho ferrites and hexagonal ferrites [3-6]. All these ferrites are noteworthy for their exceptional chemical stability, remarkable mechanical hardness, high electromagnetic strength, … etc.

$NiFe_2O_4$ fascinated researchers with its vitalizing low conductivity ferromagnetic properties and therefore low eddy current loss, abundance in nature, catalytic behavior, high electrochemical stability, … etc.

Spinel ferrite nanoparticles can be synthesized using a range of techniques, including co-precipitation, micro emulsion sol-gel, citrate sol gel, hydrothermal, the redox process, combustion, … etc. [7-10]. These synthesis methods have their own advantages and disadvantages. Santi Maensiri et al. [11] have first reported egg white method for synthesis of spinel ferrite nanoparticles, which is a cost-effective, environmentally benevolent, eco-friendly and simple method for preparing transition metal-substituted ferrites at low temperatures. Also, the toxic precursors and harmful effluents out of the reaction can also be reduced as egg white is used as precursor.

Ferrites are superior nanoparticles finding applications in practically all fields of science and technology extending from millimeter wave integrated circuitry to power handling, data storage, protective coatings and basis for lithium ion batteries, catalyst and sensors, … etc. These magnetic nanoparticles find special applications in the field of biomedicine, like drug targeting, hyperthermia and magnetic resonance imaging, … etc. owing to their elemental composition which makes them biocompatible and degradable [12-17]. Ferrites are among the effective visible light sensitive photocatalysts, as they can be used directly to harness the freely available sunlight for pollutant degradation. Keeping this view, in our present study, we made an attempt to prepare $NiFe_2O_4$ nanoparticles *via* single-step synthesis technique. In order to use it for waste water retreatment which is a driving solution for water pollution prevention. Nickel ferrite nanoparticles were already reported to be a photocatalyst for methylene blue dye with 94% efficiency [18, 19]. But till now, there is no report for $NiFe_2O_4$ nanoparticles synthesized *via* green synthesis route using egg white as fuel as a photocatalyst.

2. Experimental Procedure

2.1 Preparation

Nickel ferrite magnetic nanoparticles were made using high-chemical purity ferric nitrate nonahydrate and nickel nitrate hexahydrate along with newly prepared egg white. Egg white, rich in albumen protein- is recognized for its foaming and emulsification characteristics and is easily soluble in water, which makes it easy to combine with metal ions, while egg white is also used as a binder cum gel for material shaping [11].

Egg white and double distilled water are combined in 3:1 ratio by vigorous stirring at room temperature for one hour to form a homogeneous solution. Ni $(NO_3)_2.6H_2O$ and Fe $(NO_3)_3.9H_2O$ are taken in such a way that the corresponding composition of nickel to ferrite is 1:2 mole ratio, added dropwise to the homogeneous solution of the egg white and

strongly stirred at room temperature for four hours. No pH changes are made during the process. The mixed solution was then heated for several hours on a hot plate at 80°C, until a dried precursor was obtained. Then, the powder as synthesized was calcined for 3 hours in a muffle furnace at 600°C [20].

2.2 Characterization

The nickel ferrite nanoparticles were characterized using X-ray diffractometer, Fourier transform infrared spectroscopic analysis using KBr pellets, High-resolution Scanning Electron Microscopy, Energy Dispersive X-ray spectroscopy analysis and Vibrating Sample Magnetometer were used. The crystallite phase of the nickel ferrite was confirmed by X - ray diffraction using XPERT PRO diffractometer. The Fourier Transform Infrared analysis was recorded using Bruker IFS66V FT-IR spectrometer. The morphology of the prepared sample was studied using High Resolution Scanning Electron Microscopy. The magnetic parameter was measured using Vibrating Sample Magnetometer.

3. Results and Discussion

3.1 X-ray Diffraction Analysis

The XRD pattern of nickel ferrite nanoparticles are shown in Fig. 1. The result got from XRD data is in good agreement with the standard values of nickel ferrite (JCPDS file No: 86 – 2267). The characteristic planes at (220), (311), (400), (511) and (440) in the figure specifies the existence of cubic spinel structure. The lattice parameter of the nickel ferrite nanoparticles are found to be a = 8.337 ± 1Å using UNITCELL software [21].

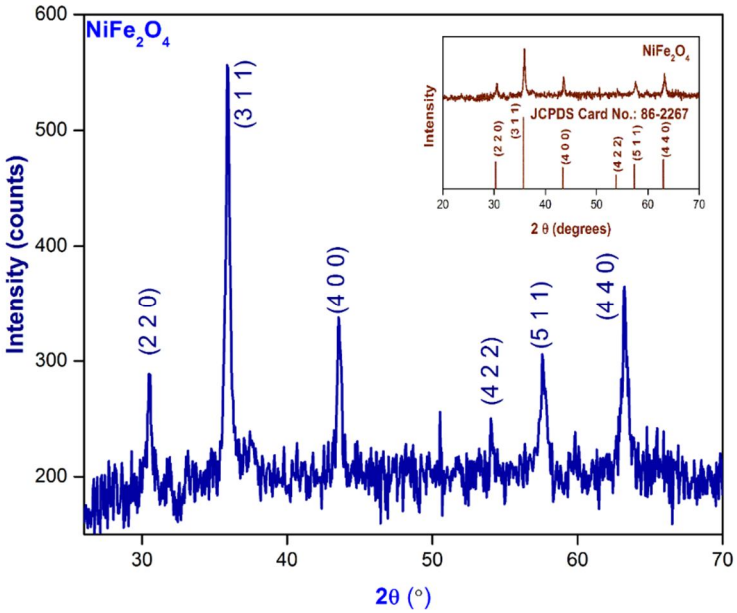

FIG. 1. XRD pattern of $NiFe_2O_4$.

Using Scherrer formula, the particle size of $NiFe_2O_4$ is calculated from the maximum intensity peak at (3 1 1) plane as 34 ± 3 nm.

$$D = \frac{k\lambda}{\beta cos\theta}$$

where 'D' is the particle size, 'λ' is the wavelength of X-ray beam used, 'β' and 'θ' represent full width half maximum and Bragg's diffraction angle of the corresponding peak, respectively and 'k' is the instrumental constant.

The X-ray density (P_x) is calculated using the following formula as 5.3020g/cc.

$$P_x = \frac{8M}{Na^3}$$

M, N and a represent molecular weight, Avagadro number and lattice constant of $NiFe_2O_4$ nanoparticles [22, 23].

Hopping lengths d_A and d_B of tetrahedral and octahedral sites are the distance between magnetic ions. d_A and d_B are calculated as d_A = 3.6291Å and d_B = 2.9632Å, respectively, using the following formulae [24]:

$$d_A = 0.25a\sqrt{3}$$

$$d_B = 0.25a\sqrt{2}$$

3.2 Fourier Transform Infrared Analysis (FT-IR) Measurement

FTIR approves the development of the spinel structure in $NiFe_2O_4$. FTIR spectrum of nickel ferrite nanoparticles are recorded in the wave number range of 4000 to 400 cm^{-1} and portrayed in Fig. 2. Two main broad metal – oxygen bands are seen in the spectrum, with the higher one (ν_1) in 589 cm^{-1} is caused by the stretching vibrations of the tetrahedral metal – oxygen [Fe–O] band, which the lower one (ν_2) in the range 419 cm^{-1} is caused by the metal – oxygen [Ni – O] vibrations in the octahedral sites [25]. The intensive wide band at 3410 cm^{-1} and less intensive one at 1574 cm^{-1} in the spectrum are owed to O–H stretching vibration intermingling through H bonds. The stretching vibration of the carboxylate group (CO_2^{2-}) is witnessed from the band at 1414 cm^{-1} and the band at 1109 cm^{-1} links to nitrate ion traces [26,27]. The values of the force constants K_T and K_O for corresponding frequencies ν_1 and ν_2 of the A-and B-sites of $NiFe_2O_4$ are calculated as 2.5379 Nm^{-1} and 1.2843 Nm^{-1}, respectively, using the formulae given below [28].

$$K_T = 4\pi c^2 \nu_1^2 \mu$$

$$K_O = 4\pi c^2 \nu_2^2 \mu$$

where, c is the velocity of light, ν_1 and ν_2 are the frequency of vibration of the A-and B-sites and μ is the reduced mass for the Fe^{3+} ions and the O^{2-} ions, which is approximately equivalent to 2.065×10^{-23}g.

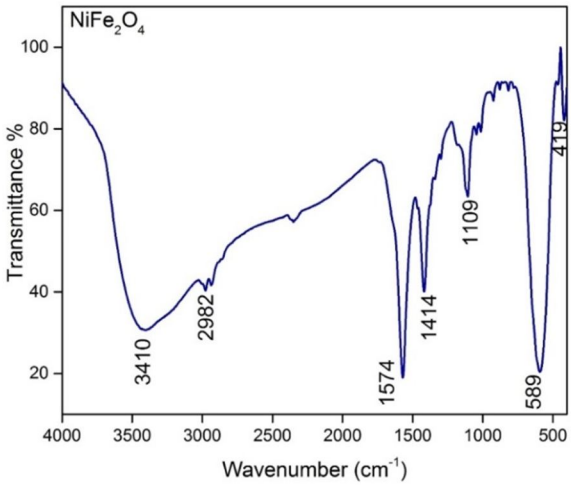

FIG. 2. FTIR spectra of $NiFe_2O_4$.

3.3 Vibrating Sample Magnetometer Analysis

From the data obtained from the Vibrating Sample Magnetometer, the magnetic property of nickel ferrite nanoparticles are analyzed. Fig. 3 illustrates the hysteresis loop for the nickel ferrite nanoparticles at room temperature. The hysteresis loop of the nickel ferrite nanoparticles is found to have less loop area which confirms the $NiFe_2O_4$ to belong to soft magnetic nanoparticles which find significance in magnetic memory devices. The magnetic moment, retentivity and coercivity of the nickel ferrite nanoparticles are 0.04319, 0.13001 emu and 137.79 G, respectively [20, 24].

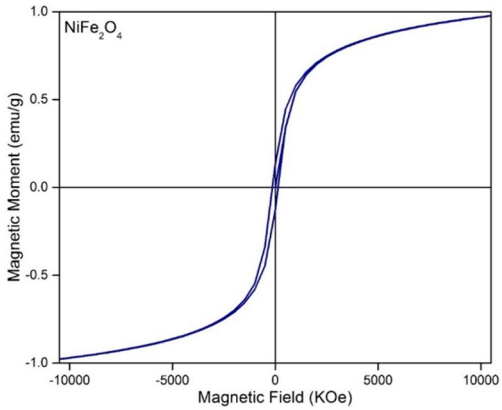

FIG. 3. Hysteresis loop of $NiFe_2O_4$.

3.4 EDX and HR-SEM Analysis

The elements present in the nickel ferrite nanoparticles are surveyed using EDX spectra. The EDX spectra of $NiFe_2O_4$ are depicted in Fig 4. The peaks at around 0.77 eV, 6.39 eV and 7 eV in the spectra support the existence of iron in the nickel ferrite nanoparticles. The peak at around 0.5 eV in the spectra discloses the existence of oxygen. The peaks at 0.85 eV, 7.47 eV and 8.2 eV in Fig. 4 narrate the existence of nickel [29].

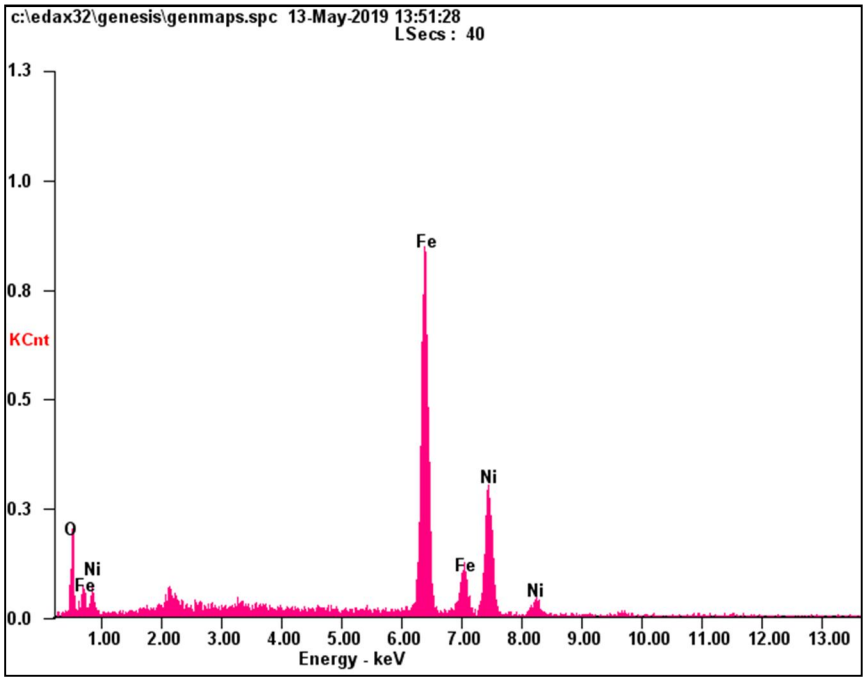

FIG. 4. EDX spectra of $NiFe_2O_4$.

The morphology of the synthesized nickel ferrite nanoparticles is recorded using HR-SEM. The HR-SEM image of $NiFe_2O_4$ at the magnification of 500 nm is represented in Fig. 5. The average particle size value was measured using ImageJ software considering as many particles as possible from the micrograph in Fig. 5 and was found to be in the range 10 to 45nm. The accumulation arises in ferrite nanoparticles owing to its magnetic nature and the binding of primary particles held together by fragile surface interactions, such as Vander Waals force. A histogram was plotted for the particle size by applying Gaussian curve to figure out the most probable value of particle size. From Gaussian fit in Fig. 5, the mean, median, maximum and minimum diameters of the $NiFe_2O_4$ nanoparticles have been determined and the values of maximum and minimum diameters are found to be 41.759 and 12.136 nm, respectively. The standard deviation of nickel ferrite nanoparticles was found to be 6.677 nm [30]. The particle size agrees well with the particle size calculated from XRD data.

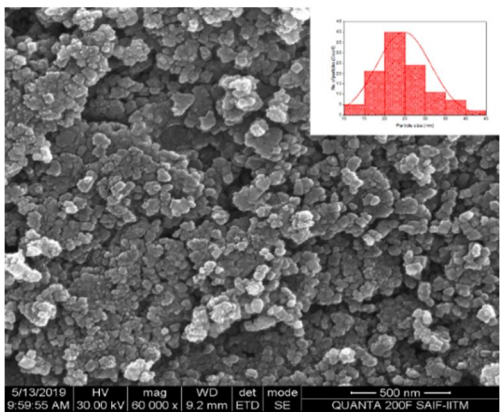

FIG. 5. Surface morphology and particle size distribution of $NiFe_2O_4$.

4. Photocatalytic Activity of Nickel Ferrite

The photocatalytic activities of nickel ferrite nanoparticles under ultraviolet light irradiation were evaluated by monitoring the decolorization of methylene blue dye. Methylene blue dye photocatalytic degradation was performed in a three-pyrex flask reactor, using $NiFe_2O_4$ nanoparticles as a photocatalyst under xenon arc lamp UV illumination (300W, Hamamatus: L 2479). 10ppm dye solution was prepared in 100ml DI water for the photocatalytic degradation of methylene blue dye, in which 0.15 g photocatalyst ($NiFe_2O_4$ nanoparticles) was added and the resulting mixture was expunged with Ar gas under continuous stirring. Consequently, the suspension obtained was balanced for 30 min to stabilize the absorption of methylene blue dye over $NiFe_2O_4$ nanoparticles before light exposure [31].

To track the process of photocatalytic degradation, the characteristic absorption of methylene blue dye at 655 nm was chosen. Fig. 6 shows a typical methylene blue dye (initial concentration: 10 mg l-1, 50 ml) photocatalytic degradation cycle using 0.05 g of the $NiFe_2O_4$ sample under UV light irradiation. With the increase in exposure time, the absorption peaks corresponding to methylene blue dye have slowly decreased.

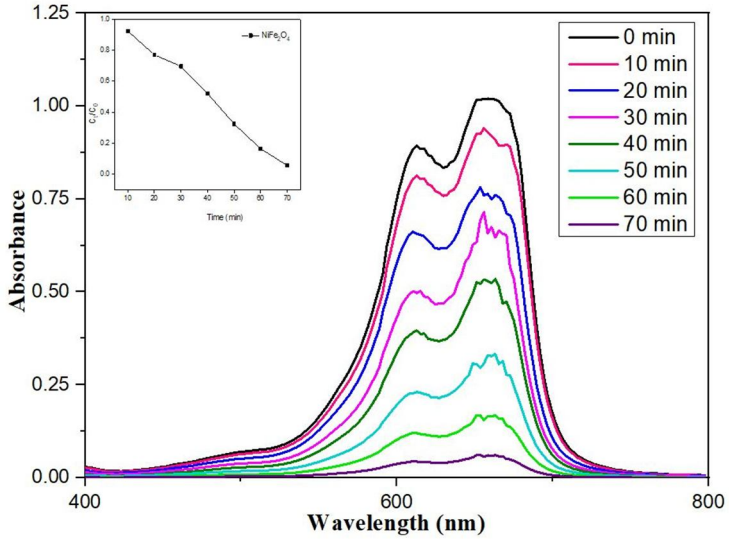

FIG.6. Absorption spectra of methylene blue dye solution in presence of $NiFe_2O_4$ photocatalyst and its degradation graph.

The photocatalytic performance of the sample with the exposure time was determined from the expression below:

$$\eta = \frac{A_o - A}{A_o} \times 100\%$$

where η is the removal efficiency, A_o is the initial absorbance and A is the variable absorbance [32].

The findings showed that the solution's absorbance decreases with increasing time intervals, suggesting that the dyes concentration decreases as exposure time increases. The degradation efficiency of $NiFe_2O_4$ photocatalyst against methylene blue is 95.6%. Thus, the nickel ferrite nanoparticles synthesized *via* the combustion process using egg white as fuel acts as an effective photocatalyst for methylene blue degradation.

5. Conclusion

The present research focused on the synthesis of nickel ferrite nanoparticles using egg white as the eco-friendly precursor *via* green synthesis path. In the auto combustion process, the egg white protein albumen was acting as fuel. The XRD results confirmed the formation of $NiFe_2O_4$ nanoparticles of nickel ferrite with a cubic spinel structure and particle size of 34 $\pm$ 3 nm. The absorption peaks in the FTIR spectra due to the vibrations of metal oxygen in 419 and 589 cm^{-1} confirms the spinel structure of nickel ferrite. The micrographs of the HRSEM showed highly agglomeration uniform spheres and the particle size to be varying from 12 to 43 nm, which is in good agreement with XRD results. The EDAX spectra clearly confirmed the existence of Ni, Fe and O in nanoparticles containing $NiFe_2O_4$. VSM was used to calculate the magnetic

parameters, such as coercivity, retentiveness and magnetic moment. The synthesized nickel ferrite nanoparticles were found to be a good photocatalyst for methylene blue dye in the ultraviolet region with efficiency of 95.6% which is more when compared to the nickel ferrite nanoparticles synthesized via chemical routes.

References

[1] Sundararajanl, M., John Kennedy, L., Nithya, P., Judith Vijaya, J. and Bououdina, M., Journal of Physical and Chemistry of Solids, 108 (2017) 61.

[2] Singhal, S., Sharma, R., Singh, C. and Bansal, S., Indian Journal of Materials Science, 2013 (2013) 1.

[3] Vinnik, D.A., Podgornov, F.V., Zabeivorota, N.S., Trofimov, E.A., Zhivulin, V.E., Chernukha, A.S., Gavrilyak, M.V., Gudkova, S.A., Zherebtsov, D.A., Ryabov, A.V., Trukhanov, S.V., Zubar, T.I., Panina, L.V., Podgornaya, S.V., Zdorovets, M.V. and Trukhanov, A.V. , Journal of Magnetism and Materials, 498 (2020) 166190.

[4] Kozlovskiy, A., Kenzhina, I. and Zdorovets, M., Ceramics International, 45 (2019) 8669.

[5] Almessiere, M.A., Trukhanov, A.V., Khan, F.A., Slimani, Y., Tashkandi, N., Turchenko, V.A., Zubar, T.I., Tishkevich, D.I., Trukhanov, S.V., Panina, L.V. and Baykal, A., Ceramics International, 46 (2020) 7346.

[6] Almessiere, M.A., Slimani, Y., Güngüneş, H., Kostishyn, V.G., Trukhanov, S.V., Trukhanov, A.V. and Baykal, A., Ceramics International, 46 (2020) 11124.

[7] Shumskaya, E.E., Kaniukov, E.Y., Vinnik, D.A., Zdorovets, M.V., Anisovich, M., Trukhanov, A.V., Tosi, D. and Molardi, C., Nanomaterials, 9 (2019) 1.

[8] Tishkevich, D.I., Korolkov, I.V., Kozlovskiy, A.L., Anisovich, M., Vinnik, D.A., Ermekova, A.E., Vorobjova, A.I., Shumskaya, E.E., Zubar, T.I., Trukhanov, S.V., Zdorovets, M.V. and Trukhanov, A.V., Journal of Alloys and Compounds, 797 (2019) 573.

[9] Almessiere, M.A., Trukhanov, A.V., Slimani, Y., You, K.Y., Trukhanov, S.V., Trukhanova, E.L., Esa, F., Sadaqat, A., Chaudhary, K., Zdorovets, M. and Baykal, A., Nanomaterials, 9 (2019) 202.

[10] Zdorovets, M.V. and Kozlovskiy, A.L., Surface and Coatings Technology, 383 (2020) 125286.

[11] Maensiri, S., Masingboon, C., Boonchom, B., Seraphin, S., Scripta Materialia, 56 (2007) 797.

[12] Trukhanov, S.V., Journal of Experimental and Theoretical Physics, 100 (2005) 95.

[13] Zdorovets, M.V. and Kozlovskiy, A.L., Vacuum, 168 (2019) 108838.

[14] Trukhanov, S.V., Troyanchuk, I.O., Pushkarev, N.V. and Szymczak, H., Journal of Experimental and Theoretical Physics, 95 (2002) 308.

[15] Trukhanov, S.V., Trukhanov, A.V., Vasil'ev, A.N., Maignan, A. and Szymczak, H., Journal of Experimental and Theoretical Physics Letters, 85 (2007) 507.

[16] Trukhanov, S.V., Khomchenko, V.A., Lobanovski, L.S., Bushinsky, M.V., Karpinsky, D.V., Fedotova, V.V., Troyanchuk, I.O., Trukhanov, A.V., Stepin, S.G., Szymczak, R., Botez, C.E. and Adair, A., Journal of Experimental and Theoretical Physics, 103 (2006) 398.

[17] Zdorovets, M.V., Arbuz, A. and Kozlovskiy, A.L., Ceramics International, 46 (2020) 6217.

[18] Mathubala, G., Manikandan, A., Arul Antony, S. and Ramar, P., Journal of Molecular Structure, 1113 (2016) 79.

[19] Adeleke, J.T., Theivasanthi, T., Thiruppathi, M., Swaminathan, M., Akomolafe, T. and Alabi, A.B., Applied Surface Science, 455 (2018) 195.

[20] Aji Udhaya, P. and Meena, M., Materials Today: Proceedings, 9 (2019) 528.

[21] https://www.esc.cam.ac.uk/research/research-groups/research-projects/tim-hollands-software-pages/unitcell.

[22] Annie Vinosha, P., Ansel Mely, L., Emima Jeronsia, J., Krishnan, S. and Jerome Das, S., Optik, 134 (2017) 99.

[23] Aji Udhaya, P., Bessy, T.C. and Meena, M., Materials Today: Proceedings, 8 (2019) 169.

[24] Nikam, D.S., Jadhav, S.V., Khot, V.M., Bohara, R.A., Hong, C.K., Mali, S.S. and Pawar, S.H., RSC Advances, 5 (2015) 2338.

[25] Raju, M.K., Chemical Science Transactions, 4 (2015) 137.

[26] Waldron, R.D., Physical Review, 99 (1955) 1926.

[27] Aji Udhaya, P., Meena, M. and Queen, M.A.J., International Journal of Scientific Research in Physics and Applied Sciences, 7 (2019) 71.

[28] Vijaya Babu, K., Satyanarayana, G., Sailaja, B., Santosh Kumar, G.V., Jalaiah, K. and Ravi, M., Results in Physics, 9 (2018) 55.

[29] https://www.edax.com/resources/interactive-periodic-table.

[30] Kumar, D., Kumar, A., Prakash, R., Singh, A.K., AIP Conference Proceedings, 2142 (2019) 070018.

[31] Vinosha, P.A., Xavier, B., Anceila, D. and Jerome Das, S., Optik, 157 (2018) 441.

[32] Pudukudy, M. and Yaakob, Z., Journal of Cluster Science, 25 (2014) 1.